Wavelet Synchro-squeezing Transform and Dynamic Threshold Supported Symmetrical Power Swing Technique for Modern Transmission Network

Monalisa Biswal[1*], *Kumar Raja Andanapalli*[1] *and Papia Ray*[2]
(1. Department of Electrical Engineering,
National Institute of Technology Raipur, Chhattisgarh 492010, India;
2. Department of Electrical Engineering,Veer Surendra Sai University of Technology,
Burla Sambalpur 768018, India)

Abstract: Distance relays are prone to symmetrical power swing phenomenon. To mitigate this issue, a dynamic threshold-supported algorithm is proposed. A single logic is not supposed to be secure for all cases. Thus, a supervisory algorithm, as proposed in this study, can aid in the improvement of the immunity of the relay during swing cases and be sensitive to symmetrical faults. In the developed stages, a three-phase power signal was used and processed in two different steps: (i) extraction of the effective intrinsic mode function (IMF) selected from the Kurtosis analysis using the wavelet synchro-squeezing transform, and (ii) estimation of the average Euclidean distance index using the absolute values of the decomposed IMF's. The adaptive threshold facilitated resistance to swing situations. At the onset of a symmetrical fault, the proposed algorithm efficiently discriminated among events using a dynamic threshold. The IEEE 39-bus test system and Indian Eastern Power Grid networks were modelled using PSCAD software, and cases were generated to test the efficacy of the method. The impact of the proposed method on a large-scale wind farm was also evaluated. A comparative analysis with other existing methods revealed the security and dependability of the proposed method.

Keywords: Distance relays, symmetrical power swing, wind farm, wavelet synchro-squeezing transform (WSST), Euclidean distance

1 Introduction

1.1 General introduction

The power swing phenomenon can arise after the power system recovers from any disturbance or heavy load disconnection. A generator outage in an interconnected area can result in swing conditions [1]. The distance relay always operates based on the impedance values measured using the local end signals. The measured impedance gradually approaches the setting characteristics following the inception of the fault. The calculation procedures for the different fault types differ from those for distance relays. The components of the -ve/zero sequence can be used to analyze an asymmetrical fault. However, during three-phase faults, only positive-sequence components are present. Moreover, the relay encounters difficulty in distinguishing symmetrical faults and symmetrical power swings (SPS) owing to its symmetrical behavior. The pattern of variations in the voltage and current signals can be the same for both events, and the impedance measured by the distance relay also faces challenges in discriminating between situations. For clear detection and discrimination of the swing phenomenon, a distance relay is employed using several methods [2]. However, in fault cases, the relay must be unblocked to attend the event. Consequently, negative, and zero-sequence components are used to address the unbalanced fault cases. The problem still lies in balanced symmetrical fault, as it does not generate any negative or zero sequence components. With a positive sequence

Manuscript received May 30, 2023; revised December 3, 2023; accepted December 19, 2023. Date of publication June 30, 2024; date of current version May 5, 2024.
* Corresponding Author, E-mail: mbiswal.ele@nitrr.ac.in
* Digital Object Identifier: 10.23919/CJEE.2024.000064

component, clear discrimination between the swing and balance faults is impossible. Previously, different methods such as time, frequency and time-frequency-based methods have been applied to address this issue.

1.2 Literature review

The instantaneous power-based method is among the various available time-domain algorithms [3]. The $\Delta P/\Delta t$ (rate of power change) method, FFT coefficient of three phase power for second order frequency component, DC value of three phase power, and conventional zero crossing detection technique output decision are integrated to unblock the relay during unbalance faults initiated following SPS. In Ref. [4], a power swing identification approach based on the moving average of phase currents was discussed. The moving average of the affected current signal in any phase is consistently positive or negative. Using these criteria, the signal and time criteria were used to detect and discriminate SPS from symmetrical faults. Authors in Ref. [5] estimated the current signal asymmetry coefficient for one power cycle, and if the value surpassed a preset threshold, the power swing blocking (PSB) function could be disabled by the relay to attend to the fault. A direct method based on the Lyapunov function for accessing the distance-relay operation during SPS was described in Ref. [6]. The duration for which the impedance lies within the trip trajectory is explained in Ref. [6]. In Ref. [7], a mathematical morphology technique based on the signal shape was presented to discern between swing and symmetrical faults. In Ref. [8], a Taylor series was applied to estimate the error-discriminating faults and swing phenomena. In Ref. [9], a distinctive feature of the differential voltage was demonstrated by obtaining the difference in time between two consecutive peaks of a voltage signal derivative. During SPS, the calculated feature always remains above a minimal value and falls below in case of a symmetrical fault. Similarly, a time-domain approach for discriminating between faults and swings was proposed in Ref. [10]. Specifically, an autoregression method was employed to calculate the voltage-current Lissajous figure deviation and estimate the Euclidean norm of the difference between the observed and predicted voltage-current points. The fault-swing discrimination value was obtained from the square root of the difference between the present value of the quarterly average of the Euclidean norm and that of one cycle.

Several frequency-domain approaches have been proposed to address this challenge. The Prony technique was used in Ref. [11] to estimate the DC component to distinguish a fault from a swing. A discrete Fourier transform based method was used in Ref. [12], to extract the fundamental frequency component and calculate the three-phase active power for swing detection. Delta values and admittance-based strategies were used in Ref. [13] to mitigate swing-fault challenges. The method proposed in Ref. [14] utilized the transient variation of dynamic phasors as a criterion to discriminate between symmetrical and asymmetrical faults from the SPS. The Fourier-Taylor transformation was used to calculate the dynamic phasor of the current signal. A phaselet method was proposed in Ref. [15] for detecting and distinguishing faults from swings using current sample estimation, and the error was computed between the actual and estimated values.

To address this problem, time-frequency-based approaches have been used by several researchers. In this context, the use of a wavelet transform (WT) to detect an SPS quickly and reliably, and distinguish it from a symmetrical fault, was demonstrated in Ref. [16]. The authors in Ref. [17] used the first and eighth decomposition levels of the voltage and current signals, and then estimated the energy of the decomposed signal for swing detection. The calculation procedure for the fault to extract high-frequency components from three-phase current signals using a wavelet packet transform with the mother wavelet db1 has been described in Ref. [18]. This index can reliably distinguish between fault and swing phenomena. In Ref. [19], a method based on online empirical mode decomposition (EMD) and the Hilbert-Huang transform (HHT) integrated approach was presented proposed to extract the amplitude and instantaneous frequency of a signal. The energy was estimated using the discrete Teager method. The energy operator functioned as a reliable index for fault detection during SPS. In Ref. [20], a technique for detecting three-phase faults during SPS by computing the Hilbert envelope from the current waveform and

applying further zero-frequency filtering was discussed. Consequently, fault-swing discrimination index was computed using the average rate of change in the amplitude of the zero-frequency filtered currents. A study considered the average sum of the current phasors with respect to time [21] to produce a trustworthy discrimination index. In Ref. [22], a method based on the apparent impedance and concentric features was proposed to identify faults and affected phases during the swing phenomenon. When the zone criterion is satisfied, the distance relay begins to estimate the apparent impedance, and the trip signal is issued.

1.3 Motivation and objective

The time, frequency, and time-frequency domain-based algorithms offer good security against swing-symmetrical fault discrimination processes. However, there are certain other critical events that may develop in a large power network, such as generator outage, large block of load switching, and sudden disconnection of a heavily loaded line. These can result in dependability issues for swing-fault detection algorithms. Therefore, a detailed analysis of all dependable cases, SPS, and symmetrical faults is essential to ensure the security and reliability of the method. The integration of a large wind farm can affect the signal quality and dynamics of the system. Therefore, an analysis of the results of wind farm integrated systems is also essential.

1.4 Contribution and paper organization

This study proposed a new methodology for symmetrical swing-fault identification. The primary objective was to identify any type of symmetrical fault initiated during both stable and unstable swing phenomena. Secure detection of symmetrical faults and maintenance of dependability during other nonfault events, such as generator outages, rerouting loads, and line disconnections was also considered. The method must be suitable for any modern power network, irrespective of the configuration, and must penetrate through renewable sources. Moreover, the algorithm must function quickly, precisely, and consistently. During the SPS, the active power has a slip-frequency component along with a nominal frequency, which does not occur during a fault. The three-phase instantaneous active power was examined in this study using the wavelet synchro-squeezing transform (WSST). The WSST was used to extract various frequency components that may be present during both the swing and fault. The average Euclidean distance (AED) was estimated using the absolute values of the extracted components. To avoid nuisance operations, a dynamic threshold value was used with the AED to discern the swing-symmetrical fault condition. Various standard power network models along with renewable-based systems were selected to verify the response of the method. Different models were simulated using EMTDC/PSCAD software, and the algorithm was validated using Matlab software. The effects of the fault distance from the relay location, fault time, and fault resistance on the effectiveness of the proposed method were confirmed and presenteds.

The remainder of this paper is structured as follows. Section 2 briefly describes the proposed approach, Section 3 analyzes the results, and Section 4 presents the conclusions.

2 Proposed methodology

In this study, a suitable signal was first considered and then analyzed to develop a reliable index for the SPS discrimination and identification of symmetrical faults. The steps for formulating the proposed index are presented below.

2.1 Selection of input signal

The swing is a well-known balance phenomenon. It contains both fundamental and slip frequencies. Therefore, the voltage and current signals during the SPS in a two-source equivalent system with two sinusoidal components can be expressed using Eqs. (1) and (2) [14].

$$v(t) = V_1 \sin\left(2\pi f_1 t + \phi_1\right) + V_2 \sin\left(2\pi f_2 t + \phi_2\right) \quad (1)$$

$$i(t) = I_1 \sin\left(2\pi f_1 t + \phi_1\right) + I_2 \sin\left(2\pi f_2 t + \phi_2\right) \quad (2)$$

where signals V_1 and V_2 and I_1 and I_2 contain the voltage and current magnitudes with frequencies f_1 and f_2, respectively, and ϕ_1 and ϕ_2 are the voltage and current phase angles for the frequencies f_1 and f_2, respectively. Three-phase instantaneous power signals

have unique features and are used as actuation signals to create relay logic as an actuation signal [14]. Under normal operating conditions of the power system, the power angle between the generator and load remains fixed. When the two areas operated at the same frequency, the power transmitted between them remained constant. The instantaneous three-phase output power using the voltage and current signals expressed in Eqs. (1) and (2) can be expressed as

$$P_{3\varphi} = v(t)\cdot i(t) = V_1 \sin\left(2\pi f_1 t + \phi_1\right) + V_2 \sin\left(2\pi f_2 t + \phi_2\right)\cdot I_1 \sin\left(2\pi f_1 t + \phi_1\right) + I_2 \sin\left(2\pi f_2 t + \phi_2\right) \quad (3)$$

During SPS, the instantaneous power oscillates and follows a sinusoidal curve. The modified form of Eq. (3) is presented in Eq. (4).

$$P_{3\varphi} = \Upsilon_1 + \Upsilon_2\left[\cos\left(\omega_1 - \omega_2\right)t\right] + \Upsilon_3\left[\sin\left(\omega_1 - \omega_2\right)t\right] \quad (4)$$

where Υ_1, Υ_2, and Υ_3 are constants. $\omega_1 = 2\pi f_1$ and $\omega_2 = 2\pi f_2$.

When a fault occurs anywhere along the transmission line during SPS, the instantaneous power in all three phases can be calculated using Eq. (5).

$$P_{3\varphi} = P_f + V_m \exp\left[-(R/L)t\right]F(t) \quad (5)$$

During a fault and power swing, the three-phase power-signal curve fluctuates, in contrast to under normal conditions. Therefore, it was selected as a useful signal for SPS detection.

2.2 **Wavelet synchro-squeezing transform** (WSST)

Separating the input signals into their time-varying spectral components facilitates in-depth studies of signal characteristics via the removal of unwanted information. The ability of a transform to represent signal components in a manner that renders them unique in the time or frequency domains is referred to as resolution. This concept encompasses both transformation localization power (i.e., the ability to discriminate between temporal and spectral information based on theoretical constraints) and the readability of depictions (i.e., any subsequent processing of the decomposition improves the spectral component separation). Finite-duration analysis windows are used in the transforms; therefore, the latter component must be adjusted to eliminate spectral leakage and smearing. Certain linear approaches are used to analyze the signal, including the short-time Fourier transform (STFT) and continuous wavelet transformation (CWT). However, all these methods are plagued by the "uncertainty principle", which states that one cannot locate a signal with arbitrary precision in either time or frequency. Studies have attempted to address this issue, with the reassignment technique (RM) being offered as a generic paradigm for improving TF representation. However, the primary problem with RM is that the reassigned transform is no longer invertible and does not agree with mode reconstruction. A phase-based method known as the "Synchro-squeezing Transform" (SST) was suggested in the field of signal analysis by Daubechies and Maes. This aims to enhance the time-scale (TS) representation provided by CWT, which is comparable to that of RM; however, it offers the added advantage of enabling mode retrieval.

The WSST is an improvement of the CWT. To enhance readability, it functions to minimize the spectrum smearing caused by a specific time-frequency transform; however, it has no influence on localization accuracy. The SST can be based on several time-frequency approaches. A WSST based on the CWT [23] was used in this study. The instantaneous frequencies of the signals are computed and reassigned when the CWT representation is established. The SST assumes that a signal can be described as the sum of harmonic components and additive noise, as mentioned in Eq. (6).

$$S(t) = \sum_{k=1}^{K} A_k(t)\cos(\theta_k(t)) + \eta(t) \quad (6)$$

where k represents the total number of signal components, A_k and K represent the amplitude and phase of the k^{th} component, and η signifies the sum of indeterminacy. The instantaneous frequency (f_k) of each component was calculated using Eq. (7)

$$f_k(t) = \frac{1}{2\pi}\frac{\mathrm{d}\theta_k(t)}{\mathrm{d}t} \quad (7)$$

Reassignment was performed exclusively along the frequency axis where most smearing occurred. At each nonzero point (a, b) in the CWT time-frequency representation $W_s(a, b)$, the relation for the instantaneous frequencies can be determined directly as

$$W_s(a,b)=\frac{-\mathrm{j}}{2\pi W_s(a,b)}\frac{\partial W_s(a,b)}{\partial b} \tag{8}$$

where j denotes an imaginary number. The smeared energy was subsequently repositioned on these instantaneous frequencies to synchro-squeeze the time-frequency representation. This was accomplished by moving the points from (b, a) to (b, $s(a, b)$). Consequently, the resulting SST representation T_s (ω_l, b), is expressed as

$$T_s(\omega_l,b)=\frac{1}{\Delta\omega}\sum_{a_k}W_s(a_k,b)\,a^{-3/2}\Delta a_k \tag{9}$$

In Eq. (9), the SST T_s (ω_l, b) is computed solely at discrete mid-range frequencies differentiated by a frequency deviation when mapping from the time-scale plane (b, a) to the time-frequency plane (b, $s(a, b)$ similarly. This is because both a and b are integer values of scale and time, respectively. The scaling step $\Delta a_k = (a_{k-1}–a_k)$ was inserted to produce distinct discrete scales a_k, and this facilitated the calculation of the wavelet decomposition $W_s(a, b)$. A finite set of modes, called intrinsic mode functions (IMFs), is extracted from the signal using the SST.

2.3 Adaptive selection scheme to extract superior IMF

Finally, after the actuating signal is processed using the WSST, the IMFs for several frequency levels for the generated scenario were retrieved. However, the selection of the optimal IMF is challenging, and this randomness affects the efficiency of the proposed approach. To circumvent this problem, an adaptive intrinsic mode function selection scheme was proposed. Considering the set of one-cycle information from the actuating signal, which is first applied to the WSST process, various IMFs were retrieved using Eq. (10)

$$\mathrm{IMF}(k,N)=\begin{bmatrix}\mathrm{IMF}(1,N)\\ \mathrm{IMF}(2,N)\\ \vdots\\ \mathrm{IMF}(k,N)\end{bmatrix} \tag{10}$$

In Eq. (10), each row contains one-cycle IMF information for a specific frequency component, and the maximum value is extracted. Among the maximum values obtained for the individual IMFs, the highest value was estimated using Eq. (11).

$$F=\max(\max(\mathrm{IMF}(1,N),\max(\mathrm{IMF}(2,N),\cdots,\max(\mathrm{IMF}(k,N))) \tag{11}$$

This process aids in the selection of a superior intrinsic mode function. This technique was repeated for each data cycle in a moving window to adaptively choose the optimal value for each interval.

2.4 Estimation of average Euclidean distance

For classification, Euclidean distance is widely employed [24-25]. In this study, the AED was calculated to distinguish symmetrical faults in the SPS. This method has a reduced computational load. Two-dimensional coordinates are used to represent the Euclidean distance, with the number of data samples (discrete data) along the abscissa and signal magnitudes along the ordinate. In relaying applications, the actuating signal is often a phasor magnitude or an instantaneously varying signal. For example, consider $A(x_i, y_i)$ and $B(x_j, y_j)$ as two consecutive points in the actuating signal. Furthermore, the Euclidean distance (ED) can be estimated at k^{th} instant using Eq. (12).

$$\mathrm{ED}(k)=\sqrt{\left(x_k-x_{k-1}\right)^2+\left(y_k-y_{k-1}\right)^2} \tag{12}$$

The ED can be estimated in a similar manner for one cycle to estimate the AED using Eq. (13) as follows

$$\mathrm{AED}(k)=\frac{\sum_{k=2}^{N}\sqrt{\left(x_k-x_{k-1}\right)^2+\left(y_k-y_{k-1}\right)^2}}{N} \tag{13}$$

where N denotes the number of samples per cycle.

This operation is repeated until the retrieved IMFs of the high-frequency component signal are exhausted. Notably, recursive windowing approach was used in this study to estimate the ED and AED values. To provide better and more accurate information, a perfect threshold is essential, or it can be adjusted dynamically. The next subsection provides an elaborate discussion on the dynamic adjustment of the threshold.

2.5 Implementation of trip signal based on threshold selection

The AED index in Eq. (13) rates the distance relay accuracy under three-phase fault and symmetric swing conditions. Although the index is close to zero during a swing and is significantly higher under fault

circumstances, distinguishing the two is challenging in certain instances. Accordingly, a trip mechanism was established, as illustrated in Eq. (14), to prevent any unintended distance relay operation.

$$\begin{cases}\text{If AED}(j) > h_{\text{dyn}} & \text{Trip signal is generated} \\ \text{Otherwise} & \text{block operation}\end{cases} \tag{14}$$

Here, h_{dyn} functioned as a low-pass filter, distinguishing the balanced three-phase fault from the SPS. The index value increased consistently whenever an abnormal event occurred in the monitored line. The commencement of transient phenomena is usually followed by the swing phenomenon, and a slip frequency (0.2-7 Hz) may result in a trustworthy situation. Based on the maximum slip frequency, the threshold value is adjusted dynamically, and the mathematical relation is expressed as Eq. (15).

$$h_{\text{dyn}} = \frac{\max(\text{Slip frequency})}{\text{Nominal frequency}} \cdot \max(\text{AED}) \tag{15}$$

The detailed procedure followed to distinguish the SPS situation from a three-phase fault is depicted in the flow diagram in Fig. 1.

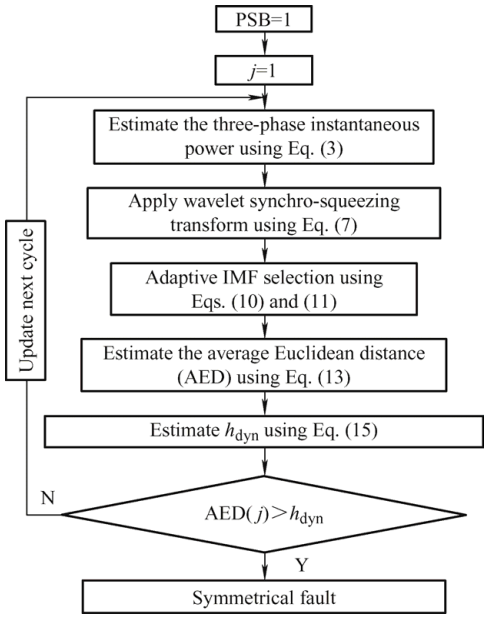

Fig. 1 Flow diagram for the proposed method

3 Simulation result

In this section, we illustrate the capabilities of the proposed dynamic threshold-based AED approach. Various power networks were considered for the simulations. For an IEEE 39 bus test system, the Indian Eastern Regional Grid (IERG) model and the renewable based modified IEEE WSCC 9-bus test system developed using EMTDC/PSCAD software were considered. The operating frequencies for all test systems were the same, that is, 50 Hz. The detailed system parameters for the IEEE 39 bus test system, shown in Fig. 2, were referred from Ref. [19]. Different SPS occurrences with varying slip frequencies were used to analyze and validate the response of the proposed method. Symmetrical faults with different fault conditions were created during SPS to verify the security of the proposed method. The method does not compromise the security attribute; thus, a dynamic threshold was used in this study to accomplish the detection and discrimination tasks. In addition, the method was tested on two distinct test systems: a real-time network and a renewable-based system, to demonstrate its flexibility and broaden the scope of its analysis. The proposed method operated with computational steps that competed with the end-point voltage and current data. A current transformer (CT) and potential transformer (PT) were used to step down the primary signal to a lower secondary value with rations of 1 000:1 A and 400 kV: 110 V.

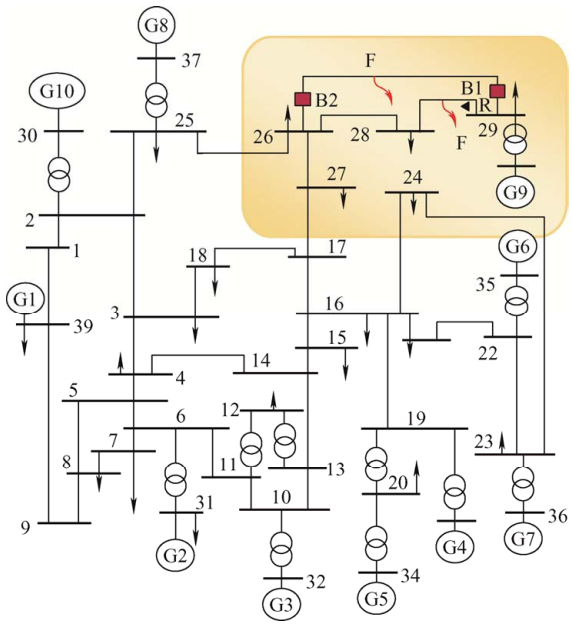

Fig. 2 IEEE 39 bus test system

The information from the instrument transformers was stepped down and used by relay *R*, which was wired close to bus-29 till the protecting line 29-28. Two different symmetrical swing phenomena: stable and unstable, were simulated using the test system.

The primary aspect of any swing-fault discrimination algorithm involves the secure identification of the initiation of a symmetrical fault during the swing-blocking period. As the PSB function enables a distance relay, the focus of the method was to continuously monitor the proposed index. If the index exceeded the dynamic threshold, a fault was detected.

On line 29-26, 100 km from bus-29, at a time of 0.8 s, a symmetrical fault (F1) was created. Owing to the imbalance between power output and load demand, the swing phenomenon occurs in practical situations. To develop the same conditions, following the occurrence of F1, the isolation times of breakers (B1 and B2) from both bus ends were delayed. Such situations were developed for both swing phenomena, and the response of relay *R* was monitored. Here, the study was based on symmetrical faults and swing phenomena; thus, the apparent impedance (Z_{app}) was estimated using positive-sequence voltage (V_1) and current (I_1) information, that is, $Z_{app} = V_1/I_1$. The value of Z_{app} was continuously monitored for symmetrical swings and faults. The sampling rate during data extraction was maintained at 1 kHz. A higher sampling rate can further increase the processor cost because a faster processor is required to store the large amount of data generated from the system when using a higher sampling rate. The primary objective of to highlight the challenges faced by SPS with the first protected zone of the distance relay. By altering the fault position on the protected line, fault onset time, and fault resistance, the performance of the proposed method was tested for both symmetrical swing phenomena.

3.1 Stable swing with different slip frequencies

In this section, we systematically analyze the reliability and security of the algorithm for different system-generated swing phenomena using the slip frequencies listed in Tab. 1. For different obtained slip frequencies (0.7-2.5 Hz) during symmetrical swing, three-phase faults were created by varying the fault position on the line, fault inception time, and fault resistance. The fault position on the line varied as 10-170 km. Various fault resistances of 0.01 Ω, 5 Ω, 50 Ω, and 100 Ω are considered. Different fault inception times were also considered to test the method. The cases highlighted in Tab. 1 were simulated, and the results are discussed below.

Tab. 1 Simulated condition for stable swing and symmetrical fault

Case	Slip frequency/ Hz	Fault conditions			
		Fault position on line/ km	Fault resistance/ Ω	Fault inception time/s	Proposed method detection time/s
1	0.7	10	100	5.42	5.427
2		100	5	4.42	4.426
3		170	100	4.78	4.787
4		60	0.01	5.56	5.566
5	1.5	150	0.01	5.65	5.658
6		80	5	4.50	4.508
7		120	100	3.65	3.657
8		100	50	4.65	4.656
9	2.5	160	0.01	2.48	2.488
10		90	5	2.55	2.556
11		140	100	2.25	2.258
12		20	50	2.65	2.656

Fig. 3a represents a simulation investigation on a 3-phase to ground fault during a slow with a slip frequency of 0.7 Hz and a fault distance of 10 km, which is extremely close to the relay position *R*. The fault commenced at 5.42 s and had a fault path resistance of 100 Ω. Similarly, in Fig. 3b, the same is depicted for a 1.5 Hz slip frequency. In this case, the fault was located 100 km from the end of the relay. Similarly, the fault resistance and time of initiation were 50 Ω, and 4.65 s, respectively.

Fig. 3 depicts the detailed response of the proposed method as well as the associated voltage, current, and relay output. Figs. 3a and 3b show the three-phase voltages, currents, and instantaneous power, AED, and trip signals for both fault cases. The predicted AED index values were below the threshold during the swing phenomenon but exceeded it after fault initiation. By using a dynamic threshold, the technique operated securely during three-phase faults and maintained its dependability throughout the swing period. Based on the other simulated cases (Tab. 1), the detection accuracy and speed of the proposed AED-index-based method were determined. For slip frequencies up to 2.5 Hz, various stable swing conditions can be detected within half a cycle of

fault inception. In addition, the fault initiation time, fault position on the line, and fault path resistance had a negligible impact on the dynamic threshold value in discriminating the symmetrical swing and fault phenomena.

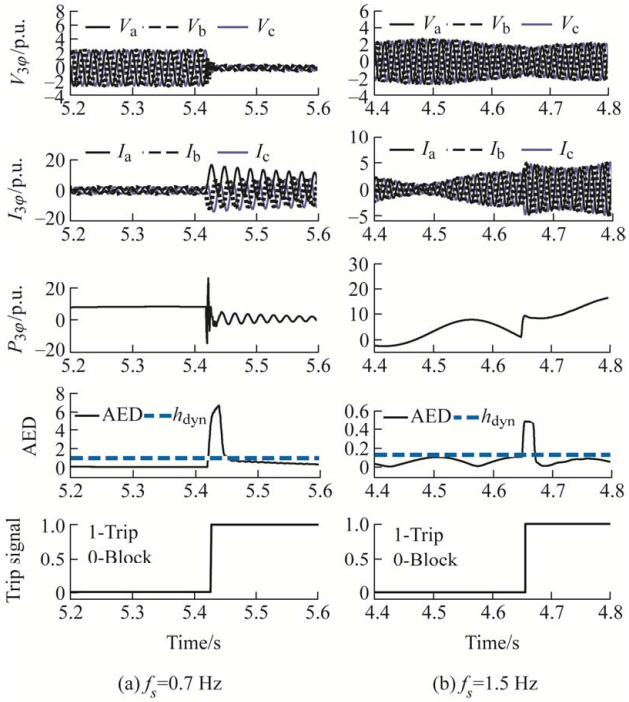

Fig. 3 Results for symmetrical faults during SPS at different slip frequencies

3.2 Unstable swing with different slip frequencies

In a manner similar to that discussed in the previous subsection, cases were developed for unstable swing phenomena. The fault scenario changed with different slip frequencies. The developed cases are listed in Tab. 2. For different slip frequencies (3.5-7 Hz) during an unstable swing, three-phase faults were created by varying the fault position on the line, fault inception time, and fault resistance. The fault position on the line varied as 10-170 km. Various fault resistances of 0.01 Ω, 5 Ω, 50 Ω, and 100 Ω were considered. Similarly, different fault inception times were considered. The cases highlighted in Tab. 2 were simulated, and the results are discussed below.

Among the simulated cases for unstable swing considering various fault positions, resistances, and inception times (Tab. 2), the 3.5 Hz and 7 Hz cases are shown in Fig. 4. The swing-blocking period continued. The impacts of a fast-swing scenario on a 3-phase to ground fault at relay position *R*, with the slip frequencies set at 3.5 Hz and 7 Hz and fault distances set at 60 km and 150 km, were investigated. For both cases the fault resistances were 50 Ω and 2 Ω.

Tab. 2 Simulated conditions for symmetrical fault during unstable swing

Case	Slip frequency/ Hz	Fault conditions			
		Fault position on line/ km	Fault resistance/ Ω	Fault inception time/s	Proposed method detection time/s
1	3.5	10	0.01	3.28	3.287
2		60	50	3.35	3.356
3		100	5	2.89	2.896
4		170	100	2.25	2.257
5	5	20	100	3.65	3.658
6		90	5	2.25	2.259
7		140	50	3.25	3.255
8		160	0.01	2.65	2.657
9	7	30	50	2.42	2.427
10		80	5	3.89	3.896
11		120	100	2.92	2.926
12		150	2	3.75	3.758

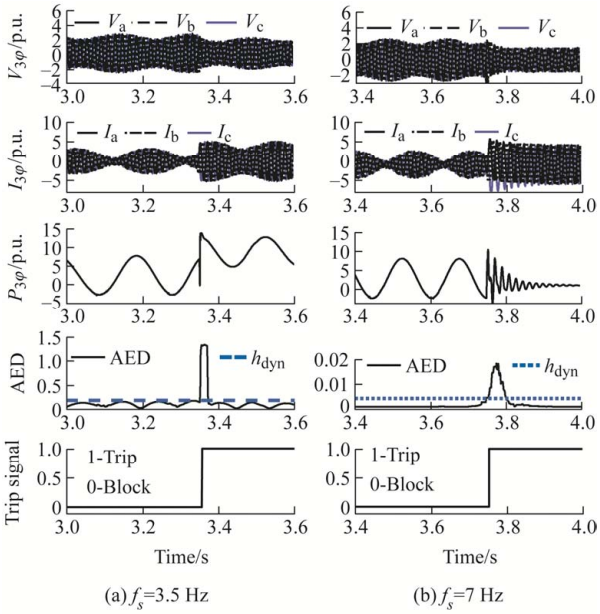

Fig. 4 Results for symmetrical faults during asymmetrical power swing at different slip frequencies

The fault initiation times, AED indices, and trip signals are shown in both subplots. For the swing phenomenon, the projected AED index value was below the threshold but exceeded it during the three-phase fault initiated under an unstable swing.

Here swing blocking period was continued with '0' output by the proposed method, as shown in the last row of both the subplots Figs. 4a and 4b. Figs. 4a and 4b subplots represent a simulation indicating that the technique operates adequately during three-phase faults and maintains security throughout swing periods with the help of dynamic threshold. Within half a cycle of fault initiation, the proposed approach detected a symmetrical fault irrespective of the type of symmetrical SPS.

3.3 Dependability and adaptability analysis

The power system may experience several different dependable situations or scenarios, during which the relay may fail to make a secure decision. This occurs only if the changes in the system parameters during the fault and no-fault scenarios are identical. To evaluate the effectiveness of the dynamic threshold-based system proposed in this study, dependable situations such as line switching, generator switching, and load switching during SPS were simulated. Voltage and current signals were recorded, and the effectiveness of the method was verified. The results are shown in Fig. 5.

Fig. 5a illustrates the performance of the line-switching phenomena occurring under SPS conditions. To showcase this, at 3.2 s, the line between buses 26 and 27 in the IEEE 39-bus test system depicted in Fig. 2 was disconnected. The line voltages, currents, three-phase instantaneous power, AED index, and trip signals generated using the proposed method are shown in Fig. 5a. The estimated AED index during the swing and line switching was very low and consistently fell below the threshold. Therefore, this method was reliable during line switching. The generator outage results are shown in Fig. 5b. This indicated another dependable case for distance relays. Therefore, to obtain a proper simulation, the response generator no. 8 (G-8) in Fig. 2 was purposely tripped at 2.55 s during swing. The three-phase voltage, three-phase current, three-phase instantaneous power, AED indices, and trip signals are shown in the subplots. The computed AED indices were completely below the threshold for swing and load switching occurrences but exceeded the threshold during three-phase fault scenarios. Even if outages occur during the swing, the proposed technique provides secure and safe operation.

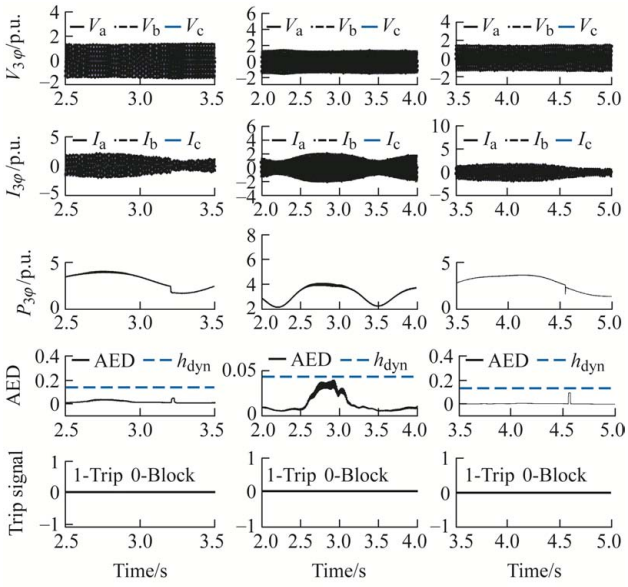

(a) Line switching (b) Generator outage (c) Load switching

Fig. 5 Performance of the proposed method for dependable situations

The load-switching phenomena in the swing state are shown in Fig. 5c. To illustrate this, a 400 MW resistive load switching operation was performed at bus 29 in the test system at 4.55 s, as illustrated in Fig. 2. The subplots show the three-phase voltage, current, instantaneous power, AED indices, and trip signals in the sequence. During swing and load-switching events, the estimated AED indices were below the threshold. This approach was effective and safe in the absence of faults.

To conduct the adaptability test, two different power system models were simulated using EMTDC/PSCAD software: (1) the IERG network and (2) a renewable-based modified IEEE WSCC 9-bus test system.

3.4 Indian Eastern Regional Grid (IERG) network

The IERG model as shown in Fig. 6 with system parameters considered from Ref. [26], was used to validate the technique. The reliability and security of the protective relays under generator shutdown and symmetrical fault circumstances during fast-swing scenarios were considered for the simulation.

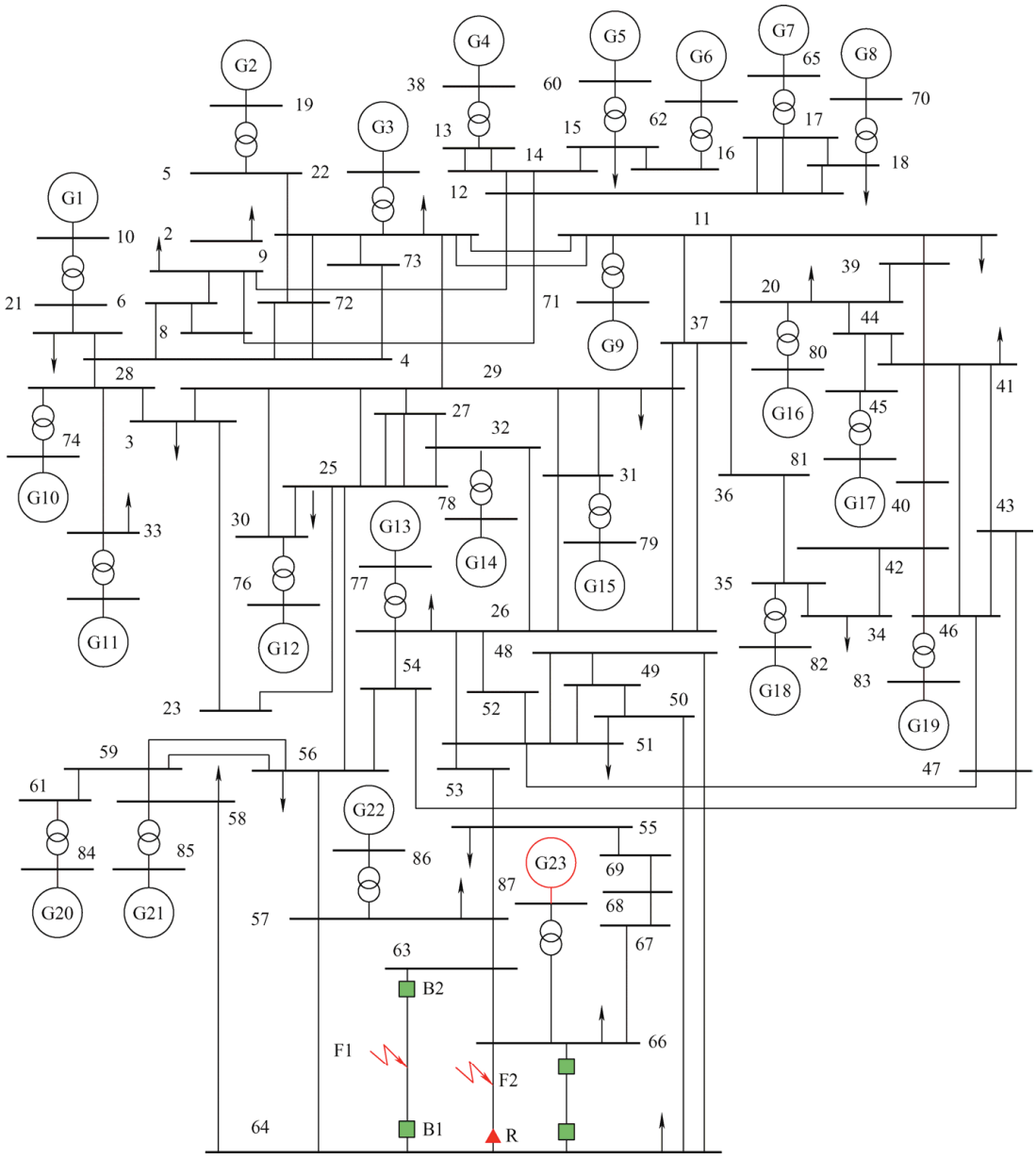

Fig. 6 A 400 kV Indian Eastern Regional Grid (IERG)

At 0.8 s on the middle line between buses 63 and 64, a three-phase fault (F1) was initiated to simulate a generator failure during the swing phenomenon. The line was isolated after 0.35 s by switching between breakers B1 and B2. As indicated by the relay (*R*) protecting line 64-63, the system generated a swing phenomenon as a result of delayed tripping. Generating unit 23 (G-23) was tripped deliberately at 4 s during the swing. The first row in Fig. 7a shows the impedance trajectories for both the swing and generator failure conditions. Because the trajectories for both scenarios were inside the setting zone, it was impossible to distinguish between the swing and generator failures. Three-phase voltage and current plots are shown in the second and third rows of Fig. 7a, respectively. The proposed AED index and trip signal are shown in the fourth and fifth rows of Fig. 7a, respectively. The AED was extremely low and well below the threshold for both swing and generator failures. The proposed method can be used to preserve relay dependability by preventing relay failures in dependable situations.

For security analysis, at 3.356 s, a symmetrical fault (F2) was generated on lines 64-66 with a fault resistance of 10 Ω. Fig. 7b depicts the results.

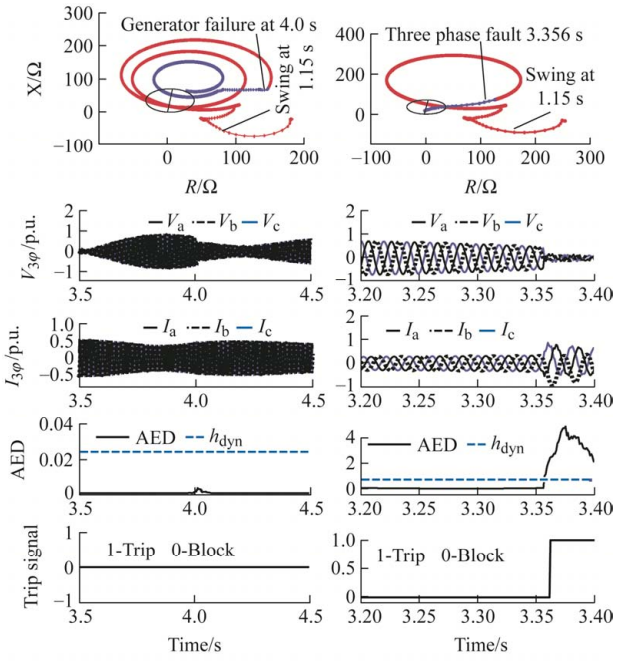

(a) Generator failure (b) Three-phase fault

Fig. 7 Result of proposed method during unstable swing

The index was initially below the threshold during the swing and increased above it at the onset of the fault. During an unstable swing, the IERG system can detect fault at 3.36 s. The responses of the AED index and relay output are shown in Fig. 7b. Therefore, this method can make trustworthy decisions when applied to large real-power networks. A previous study has shown that the proposed technology is secure and reliable, and that it can identify and isolate any symmetrical faults in the protected portion from the SPS.

3.5 Renewable based modified IEEE 9-bus WSCC system

An integrated renewable WSCC 3-machine 9-bus system model was used to assess the effectiveness of the suggested approach [27]. In this study, a wind farm (WF) was defined as a large collection of wind turbines that collectively produced 5 MW using DFIG technology [28]. Individual wind turbine ratings can range as 1.5-5 MW, depending on the manufacturer and other factors. Fig. 8 shows that the power system model after Generator-3 was replaced with a DFIG-based WF and a 100 MW AC/DC/AC IGBT-based PWM converter. The model parameters for the 400 kV transmission line linking the 100 MW WF can be found in Ref. [29] (which includes twenty 5 MW wind turbines). To test the efficacy of the proposed method, a modified IEEE 9-bus WSCC was considered (400 kV, 50 Hz), as illustrated in Fig. 8.

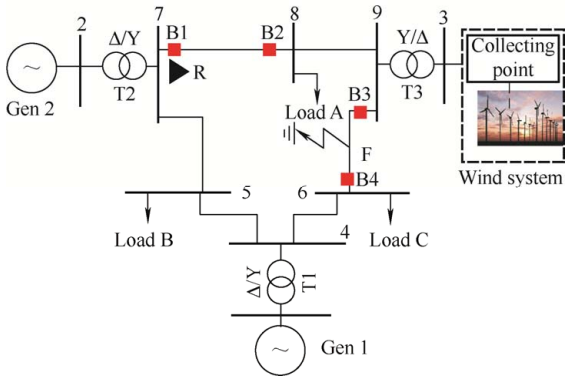

Fig. 8 Renewable-based modified IEEE 9-bus WSCC system

To study the swing phenomenon, a three-phase fault (F) in the line between buses 9-6, which was 155 km from bus 9, was created at 1.0 s. The fault can be cleared by opening breakers B3 and B4. Owing to a lag in the fault clearance process, the distance relay R at bus-7 experienced a swing phenomenon. A symmetrical fault was then generated on line 7-8 beneath the first zone of relay R under slow- and fast-swing conditions. The samples were collected at a frequency of 840 Hz. A three-phase fault was simulated in line 7-8 with fault inception time of 3 s, fault resistance of 1 Ω, and fault distance of 60 km, during a fast SPS. Fig. 9 shows the results of the

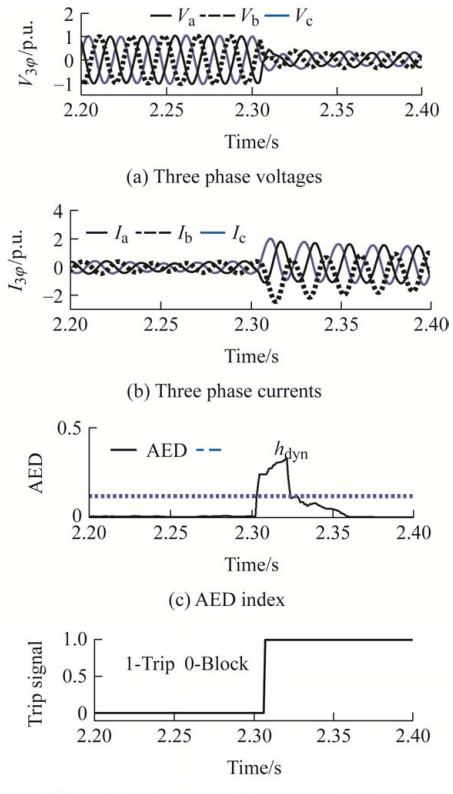

(a) Three phase voltages

(b) Three phase currents

(c) AED index

(d) Trip signal generated by proposed method

Fig. 9 Results for symmetrical fault during unstable swing for wind integrated network

proposed method. The subplots show the three-phase voltage, three-phase currents, AED indices, and trip signals. The estimated AED indices were below the threshold during the swing phenomenon; however, the three-phase fault scenario surpassed the threshold. The index exceeded goes above the threshold and remained constant for several cycles. Consequently, after 7.5 ms of detection time, the relay sent a tripping command.

3.6 Comparative analysis

To determine how the suggested strategy performed better than the alternative approaches in accomplishing tasks, a comparative analysis was conducted. Two methods, the moving window average technique (MWA) [4] and average rate of change of current (ARCC) [21], were considered as Method-1 and Method-2 to compare the responses of each method with the proposed method for line switching during the unsymmetrical power swing case. To differentiate between faults and swings, Method-1 combined sign and time criterion analyses. In this method, the fault discrimination threshold was $3N/4$, and the swing discrimination threshold was $N/2+1$. In this scenario, N was the largest number that could be calculated by adding the estimated average sum of the positive and negative phases. Swing requires both the positive and negative sign conditions to be greater than zero, whereas a fault requires only a positive sign condition. Again, the time requirements were above the fault threshold and below the swing threshold. Each phase had its own set of limits based on the magnitudes of the fault currents. Power swing and three-phase faults can be easily distinguished using the calculated index values.

Method-2 employed the ARCC. In this method, a density functional theory (DFT)-based technique was used to first estimate the current phasor, which was then used to determine the differential phase current with respect to time. To acquire a secure index for fault detection, the average rate of change of the current was computed for each time step of duration $T_s/4$ for all phases. T_s is the power-frequency cycle. Finally, the ARCC index values were obtained by selecting the maximum value among the ARCC computed for all phases for each time-step interval. During the swing phenomenon, the estimated ARCC index values were nearly zero, with substantial changes occurring in the symmetrical fault event. A fixed threshold was used to categorize the events.

A 400 kV, 50 Hz IEEE 39 bus test configuration (Fig. 2) was used for comparison. Power fluctuations that caused line switching were modelled within the EMTDC/PSCAD environment. In this case study, a comparison was made between Methods-1, -2, and the proposed method for the line-switching operation during swing. A symmetrical fault (F1) was initiated at 0.8 s on line between 29-26, 100 km from bus-29, associated with swing phenomena. In practice, a swing occurs in case of a mismatch between the supply and demand. Because of the delayed fault-clearance process, the system was unstable. This study considered the issue in the first zone of a distance relay (R) associated with a 29-28 bus. A line-switching procedure was considered between buses 26 and 25. The line breaker for bus number 26 tripped at 3.22 s. The responses of the different methods are shown in Fig. 10.

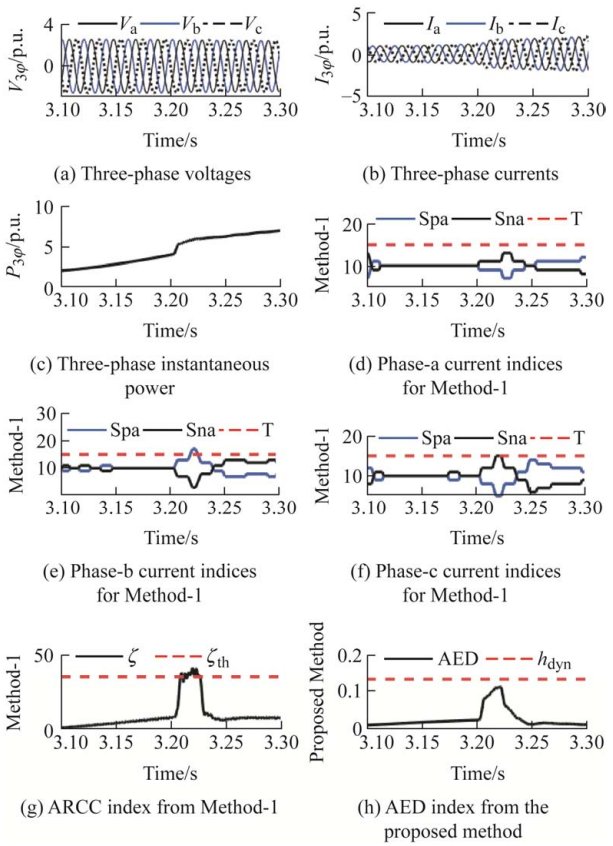

Fig. 10 Comparative assessment results for the line-switching transient during an asymmetrical power swing

All existing methods compute indices that are influenced by line switching and swing phenomena.

However, the results of Method-1 and Method-2 were accurate. The swing scenario validated for the indices of Method-1 and -2 respectively; however, the line-switching scenario rendered them invalid. The results of Method-1 are shown in Figs. 10d-10f. Similarly, the responses of Method-2 and the proposed methods are shown in Figs. 10g, 10h. The proposed AED index was correct because it was less than the threshold both during swing and after line switching. The proposed method was effective for the swing and line switching scenarios. Therefore, the proposed method is safe, dependent, and secure.

4 Conclusions

To ensure accurate relay judgement, this study proposed a novel balanced three-phase fault and symmetrical swing detection and discrimination mechanism. Using the WSST, a signal processing method, the IMFs of the three-phase instantaneous power signal were extracted. The advantages of the proposed method are as follows.

(1) It adaptively selected superior IMF characteristics and used a dynamic threshold.

(2) The AED index was estimated to provide a useful and dependent index. The index was zero for a symmetrical power swing and only increased above the threshold when a symmetrical fault was initiated.

(3) The procedure is simple and provides rapid results.

(4) The procedure can be completed without additional signal filtration or complex mathematical operations.

(5) The efficacy of the method was evaluated using the results obtained from an IEEE 39 bus test system operating at 400 kV and 50 Hz.

(6) This approach is feasible for application in any renewable-energy-based power network.

(7) The proposed approach can be used for any electricity network without being affected by the threshold selection process. Therefore, it can be used as a supervisory algorithm with distance relay to reduce the percentage of future blackouts.

References

[1] IEEE Power System Relaying Committee of the IEEE Power Engineering Society. Power swing and out-of-step considerations on line, Report PSRCWGD6, July 2005.

[2] P Kundur. Power system stability and control. New York: McGraw-Hill, 1994.

[3] B Mahamedi, J E Fletcher. Setting free method for detection of asymmetrical faults during power swing. *Electric Power System Research*, 2020, 181: 1-11.

[4] J G Rao, A K Pradhan. Power swing detection using moving averaging of current signals. *IEEE Transactions on Power Delivery*, 2015, 30(1): 368-376.

[5] C Lazaro, J P Marques, G Marchesan, et al. Waveform asymmetry of instantaneous current signal based symmetrical fault detection during power swing. *Electric Power System Research*, 2018, 155: 340-349.

[6] V Azbe, R Mihalic, J Jaeger. A direct method for assessing distance-protection behavior during power swings. *International Journal of Electrical Power & Energy System*, 2017, 90: 94-102.

[7] S Gautam, S M Brahma. Out of step blocking function in distance relay using mathematical morphology. *IET Generation Transmission & Distribution*, 2012, 6(4): 313-319.

[8] I Tekdemir, B Alboyaci. A novel approach for improvement of power swing blocking and deblocking functions in distance relays. *IEEE Transactions on Power Delivery*, 2017, 32(4): 1986-1994.

[9] B Patel. A new technique for detection and classification of faults during power swing. *Electric Power System Research*, 2019, 175: 1-10.

[10] B Patel, P Bera, S H N Dey. Differential voltage-based fault detection during power swing. *IET Generation Transmission & Distribution*, 2020, 14(1): 157-165.

[11] S Lotfifard, J Faiz, M Kezunovic. Detection of symmetrical faults by distance relays during power swings. *IEEE Transactions on Power Delivery*, 2010, 25(1): 81-87.

[12] B Mahamedi, J G Zhu. A novel approach to detect symmetrical faults occurring during power swings by using frequency components of instantaneous three-phase active power. *IEEE Transactions on Power Delivery*, 2012, 27(3): 1368-1375.

[13] S M Hashemi, M S Pasand, M Shahidehpour. Fault detection during power swings using the properties of fundamental frequency phasors. *IEEE Transactions on Smart Grid*, 2019, 10(2): 1385-1394.

[14] J Khodaparast, M Khederzadeh. Three-phase fault detection during power swing by transient monitor. *IEEE*

Transactions on Power Delivery, 2015, 30(5): 2558-2565.

[15] M M Ghalesefidi, N Ghaffarzadeh. A new phaselet-based method for detecting the power swing in order to prevent the malfunction of distance relays in transmission lines. *Energy Systems*, 2021, 12: 491-515.

[16] S M Brahma. Distance relay with out-of-step blocking function using wavelet transform. *IEEE Transactions on Power Delivery*, 2007, 22(3): 1360-1366.

[17] S M Akolkar, H R Jariwala. An advanced transmission line protection algorithm to detect power swing and fault using speedy wavelet. *Iranian Journal of Science and Technology*, 2022, 46: 701-711.

[18] B Patel, P Bera. Fast fault detection during power swing on a hybrid transmission line using wavelet packet transform. *IET Generation Transmission & Distribution*, 2019, 13(10): 1811-1820.

[19] S Biswal, M Biswal. Fault-swing discrimination using hilbert-haung transform integrated discrete teager kaiser energy operator. *IET Science Measurement & Technology*, 2018, 12(7): 829-837.

[20] M S Prabhu, P K Nayak, G Pradhan. Detection of three-phase fault during power swing using zero frequency filtering. *International Transactions on Electrical Energy Systems*, 2019, 29(1): 1-15.

[21] K Andanapalli, M Biswal. Symmetrical fault-swing discrimination algorithm for transmission system. *Journal of Institution of Engineers*, *Series B*, 2021, 102: 1033-1048.

[22] M Arumuga, M J B Reddy. Distance protection methodology for detection of faulted phase and fault along with power swing using apparent impedance. *IEEE Access*, 2022, 10: 43583-43597.

[23] J B Tary, R H Herrera, M V D Baan. Analysis of time-varying signals using continuous wavelet and synchrosqueezed transforms. *Philosophical Transactions Series A Mathematical*, *Physical and Engineering Sciences*, 2018, 376(2126): 1-16.

[24] S Gao, X Ren, Y Zhang. Improvement of multi-objective evolutionary algorithm and optimization of mechanical bearing. *Engineering Application of Artificial Intelligence*, 2023, 120: 105889.

[25] C D Prasad, P K Nayak. A DFT-ED-based approach for detection and classification of faults in electric power transmission networks. *Ain Shams Engineering Journal*, 2019, 20(1): 171-178.

[26] Eastern Regional Power Committee (ERPC). Annual Reports, 2017. http://erpc.gov.in/wp-content/uploads/2018/06/zAnnual-Report-2017-18-1.pdf.

[27] P K Nayak, A K Pradhan, P Bajpai. A fault detection technique for the series-compensated line during power swing. *IEEE Transactions on Power Delivery*, 2013, 28(2): 714-722.

[28] J Jonkman, S Butterfeld, W Musial, et al. Definition of a 5-MW reference wind turbine for offshore system development, NREL/TP-500-38060. Golden, CO: National Renewable Energy Laboratory, 2007: 1-75. https://doi.org/10.2172/947422.

[29] A Y Goharrizi, D Muthumuni, Y Pipelzadeh. Modeling of type-3 wind farm and investigation of fault contribution in power system. *IEEE Power and Energy Society General Meeting (PESGM)*. Boston, MA, 2016: 1-5.

Monalisa Biswal (S'12-M'13-SM'20) received Ph.D. degree in Electrical Engineering from Sambalpur University in 2013. Currently she is working as an Assistant Professor in the Department of Electrical Engineering, NIT Raipur, India. Her area of interest includes power system protection.

Kumar Raja Andanapalli received his Ph.D. degree in Electrical Engineering from NIT Raipur in the year 2023. Presently, he is an Assistant Professor in the EEE department in SRKR Engineering College, AP. His area of interest includes power system protection.

Papia Ray (S'11-M'14-SM'19) received her Ph.D. degree from IIT Delhi in 2013. She is currently serving as an Associate Professor and Head of Electrical Engineering Department of Veer Surendra Sai University of Technology, Burla, Odisha. She has 20 years of teaching experience. Her areas of interest include power system protection, wide area measurement, power quality, load forecasting, and biomedical signal processing.